Supporting Information

Circularly Polarized Luminescence of Eu(III) Compounds with chiral BINOL-derived Bisphosphate Ligands

Carlo Andrea Mattei,[1] Kais Dhbaibi,[1] Bertrand Lefeuvre,[1] Vincent Dorcet,[1] Gilles Argouarch,[1] Olivier Cador,[1] Boris Le Guennic,[1] Olivier Maury,[2] Claudia Lalli,[1] Stéphan Guy,[3] Amina Bensalah-Ledoux,[3] François Riobé,*[2] Bruno Baguenard,*[3] Fabrice Pointillart*[1]

[1] Univ Rennes, CNRS, ISCR (Institut des Sciences Chimiques de Rennes) – UMR 6226, 35000 Rennes (France)

E-mail: fabrice.pointillart@univ-rennes1.fr

[2] Univ Lyon, Ens de Lyon, CNRS UMR 5182, Université Claude Bernard Lyon 1, Laboratoire de Chimie, 69342, Lyon (France)

E-mail: francois.riobe@ens-lyon.fr

[3] Univ Lyon, Université Claude Bernard Lyon 1, CNRS, UMR 5306, Institut Lumière Matière, 69622 Lyon (France)

E-mail: bruno.baguenard@univ-lyon1.fr

{[Dy(hfac)$_3$((*S*)-L^3)]$_3$}$_n$: 32.8 mg (0.04 mmol) of [Dy(hfac)$_3$(H$_2$O)$_2$] were added to a solution of 30.3 mg (0.04 mmol) of (*S*)-L^3 or (*R*)-L^3 in 5 mL of CH_2Cl_2. After 15 minutes of stirring, 30 mL of *n*-hexane were layered. After several days, the solution was slowly evaporated leading to a colourless and microcrystalline solid. 27.6 mg, 44 % yield for {[Dy(hfac)$_3$((*S*)-L^3)]$_3$}$_n$. Anal. calcd (%) for $C_{177}H_{129}Dy_3F_{54}O_{42}P_6$: C 45.90, H 2.79; found: C 45.82, H 2.94. Representative I.R. (KBr, range 3200–400 cm^{-1}): 3079 (w), 2937 (w), 2863 (w), 1654 (s), 1591 (w), 1555 (m), 1527 (m), 1491 (s), 1256 (s), 1201 (s), 1147 (s), 1102 (m), 1075 (m), 1027 (m), 1018 (m), 992 (m), 971 (w), 962 (w), 808 (w), 798 (m), 778 (w), 755 (m), 741 (w), 687 (w), 661 (m), 586 (m), 529 (w), 507 (w) and 466 (w) cm^{-1}. Slow evaporation from a solution in

CH_2Cl_2/*n*-hexane led to single crystals suitable for structural X-ray studies. $[\alpha]_D^{25} = -6.5$ for $\{[Dy(hfac)_3((S)\text{-}L^3)]_3\}$ (c = 1.0, $CHCl_3$).

It crystallizes in the $P2_12_12_1$ (N°19) chiral orthorhombic space group (Table S2) and its asymmetric unit is composed of three **(*S*)-L^3** ligands and three $Dy(hfac)_3$ moieties. The $Dy(hfac)_3$ moieties are linked by the **(*S*)-L^3** ligands through the P=O groups to form a one-dimensional structure (Figure S1). The Dy(III) ion is surrounded by eight oxygen atoms coming from three $hfac^-$ anions and two P=O groups. The arrangement of the ligands leads to distorted square antiprism (D_{4d} symmetry) coordination polyhedron for the three crystallographically independent Dy(III) centres. The deviation from the ideal symmetries are determined by SHAPE[1] analysis and depicted in Table S3. From such analysis, it appears that the Dy1 and Dy3 adopt an almost regular square antiprism while the coordination sphere of Dy2 is close to a D_{2d} symmetry (triangular dodecahedron). The average Dy-O bond length is (2.34(6) Å) and the Dy-O_{hfac} are slightly longer than the Dy-$O_{P=O}$ bond lengths. The $_{P=O}$O-Dy-$O_{P=O}$ angles range from 139.9° to 152.8°. The angle between the planes formed by the binaphtyl groups are found close in the three **(*S*)-L^3** ligands of the asymmetric unit with values ranging from 75.0(3)° to 86.0(1)°. The intra-chain Dy-Dy distances are found equal to 12.528(2) Å (Dy1-Dy2), 12.339(2) Å (Dy2-Dy3) and 12.662(3) Å (Dy3-Dy1). The crystal packing (Figure S2) highlights both F···F and H···F contacts to assume the cohesion of the crystal but no π-π stacking has been found. The shortest inter-chain Dy-Dy distances are found equal to 11.447(2) Å (Dy1-Dy1) so slightly shorter than the intra-chain distances.

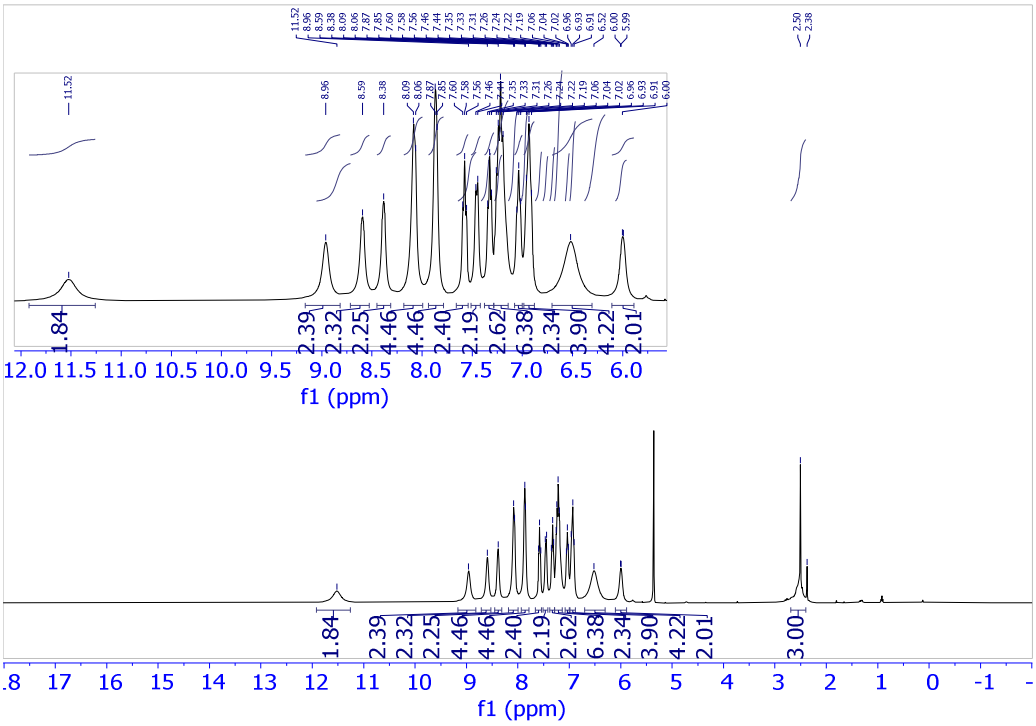

Figure S1. ^{1}H NMR spectrum of **[(*S,S,S*)/(*R,R,R*)-2]** in CD_2Cl_2 at 298 K (400 MHz). Inset: expanded region from 5.56 to 12.06 ppm.

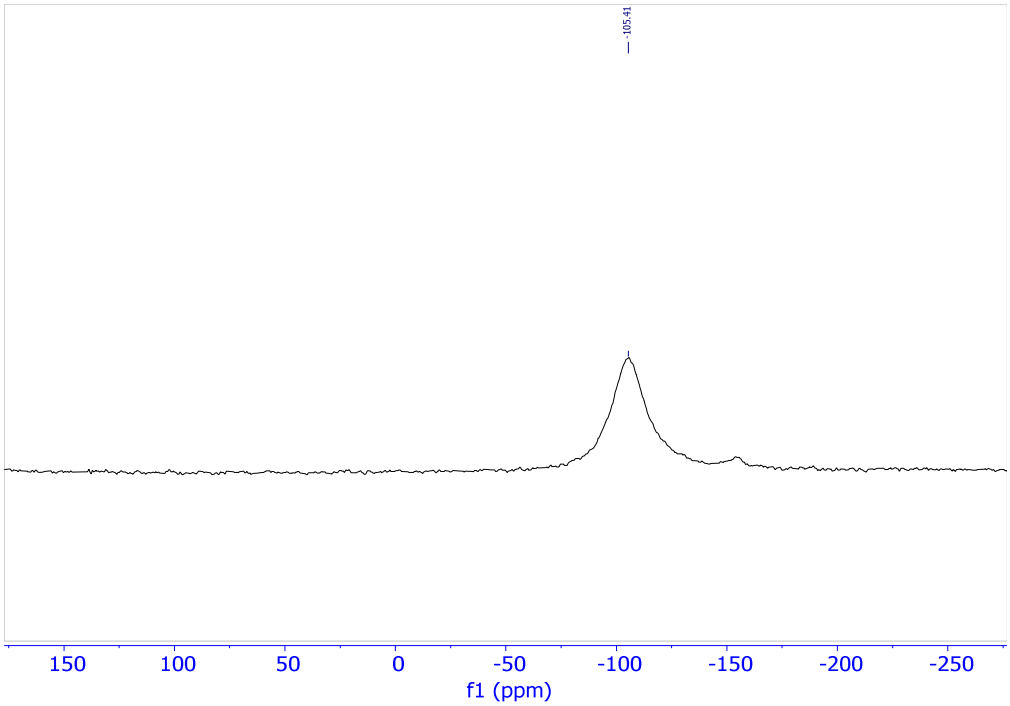

Figure S2. ^{31}P spectrum of **[(*S,S,S*)/(*R,R,R*)-2]** in CD_2Cl_2 at 298 K (162 MHz).

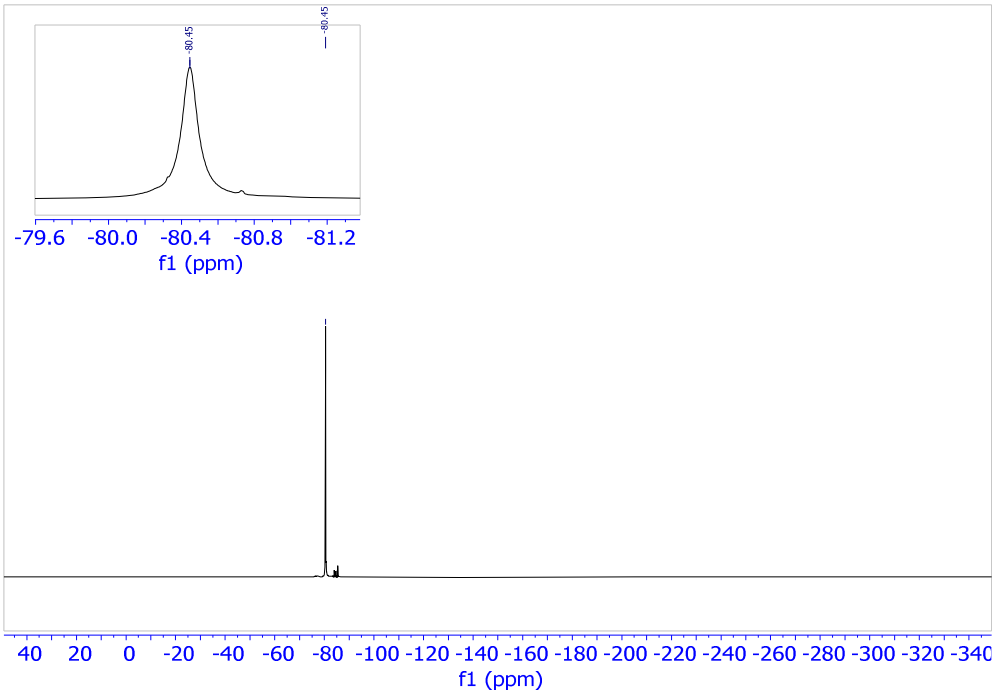

Figure S3. ^{19}F spectrum of **[(*S,S,S*)/(*R,R,R*)-2]** in CD_2Cl_2 at 298 K (376 MHz). Inset: expanded region from -81.3 to -79.6 ppm.

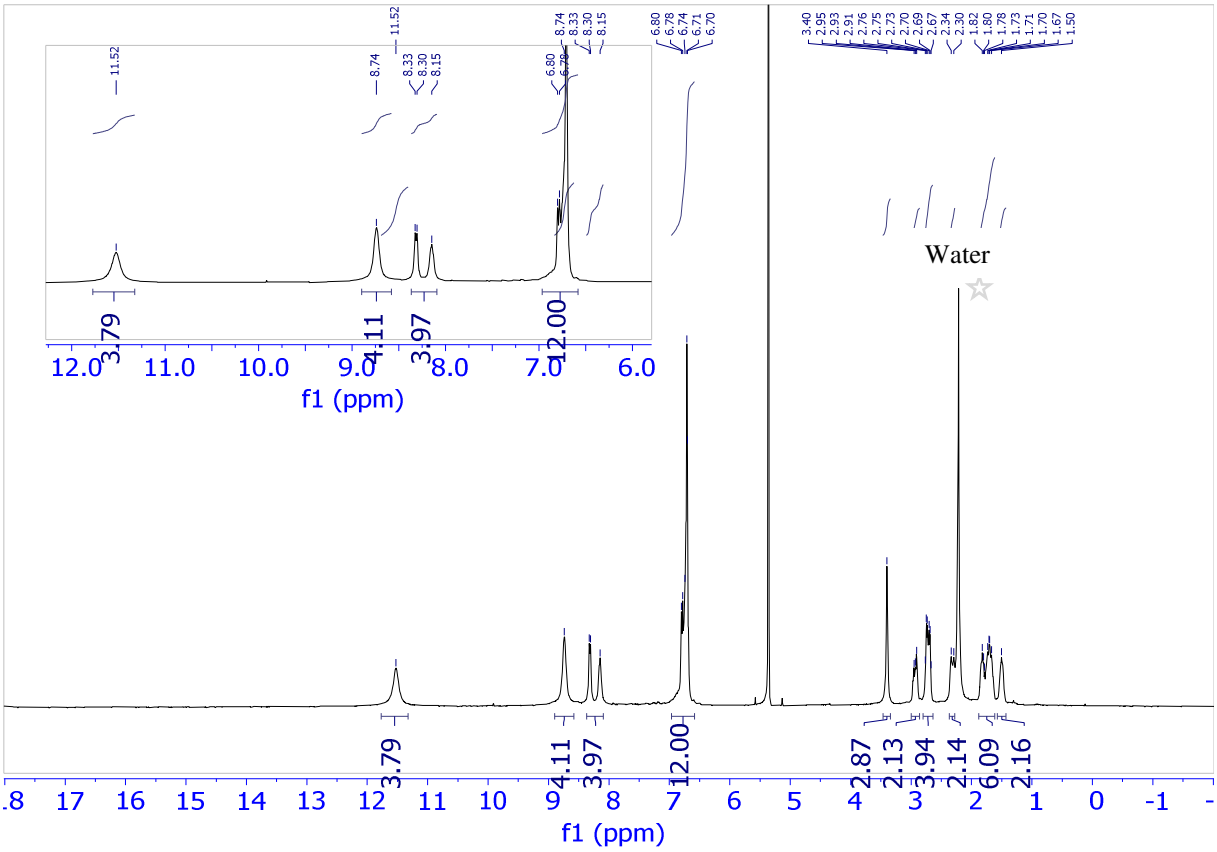

Figure S4. ^{1}H NMR spectrum of **[(*S*)/(*R*)-3]** in CD_2Cl_2 at 298 K (400 MHz). Inset: expanded region from 5.80 to 12.22 ppm.

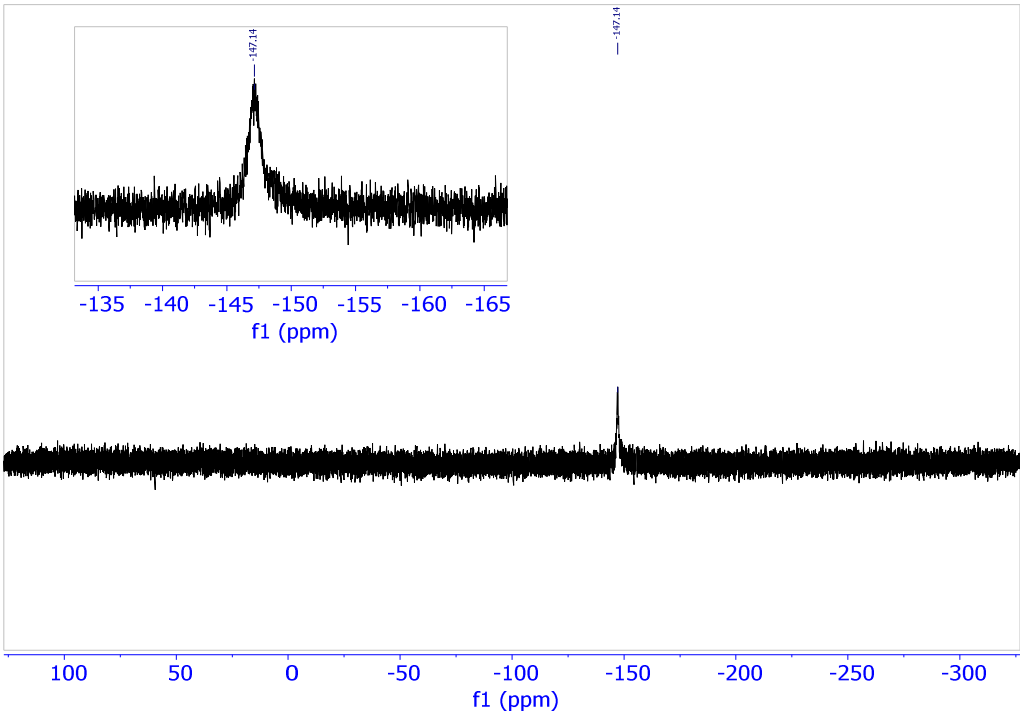

Figure S5. ^{31}P spectrum of **[(*S*)/(*R*)-3]** in CD_2Cl_2 at 298 K (162 MHz). Inset: expanded region from -166 to -135 ppm.

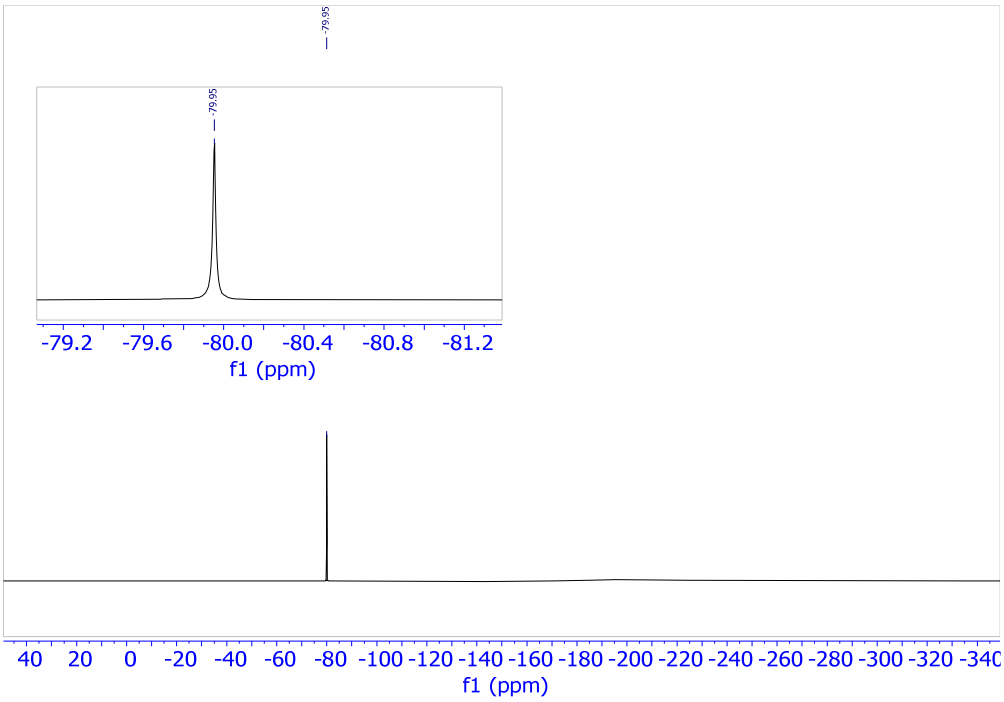

Figure S6. ^{19}F spectrum of **[(*S*)/(*R*)-3]** in CD_2Cl_2 at 298 K (376 MHz). Inset: expanded region from -81.4 to -79.1 ppm.

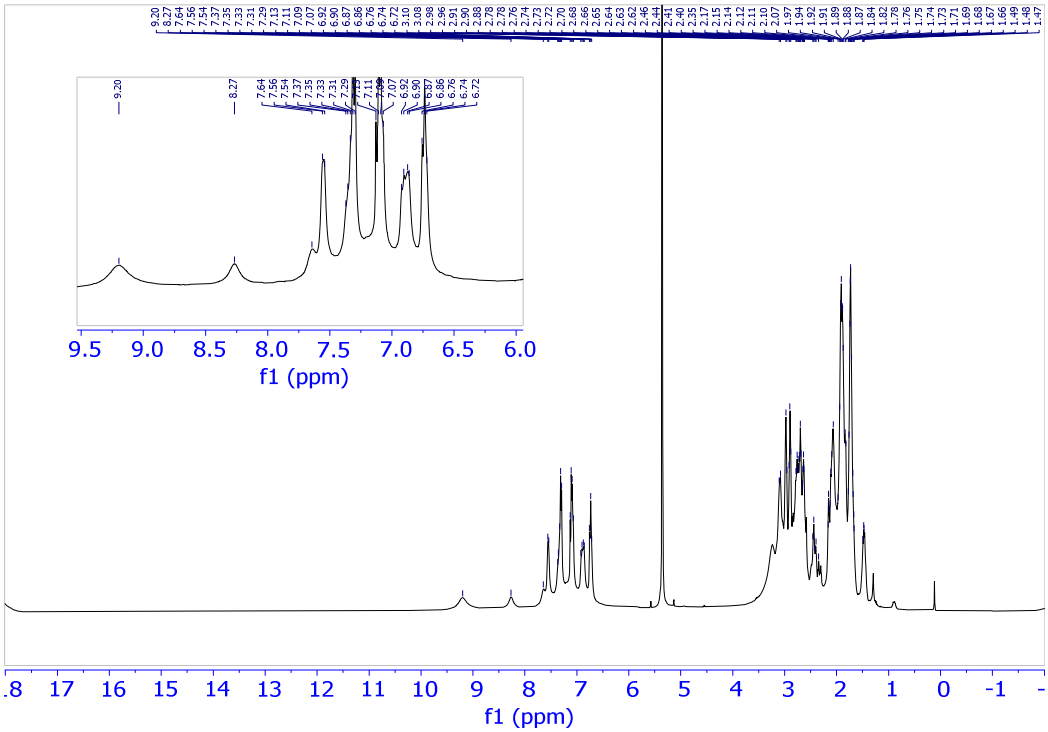

Figure S7. ^{1}H NMR spectrum of **[(*S,S,S*)/(*R,R,R*)-4]** in CD_2Cl_2 at 298 K (400 MHz). Inset: expanded region from 5.98 to 9.52 ppm.

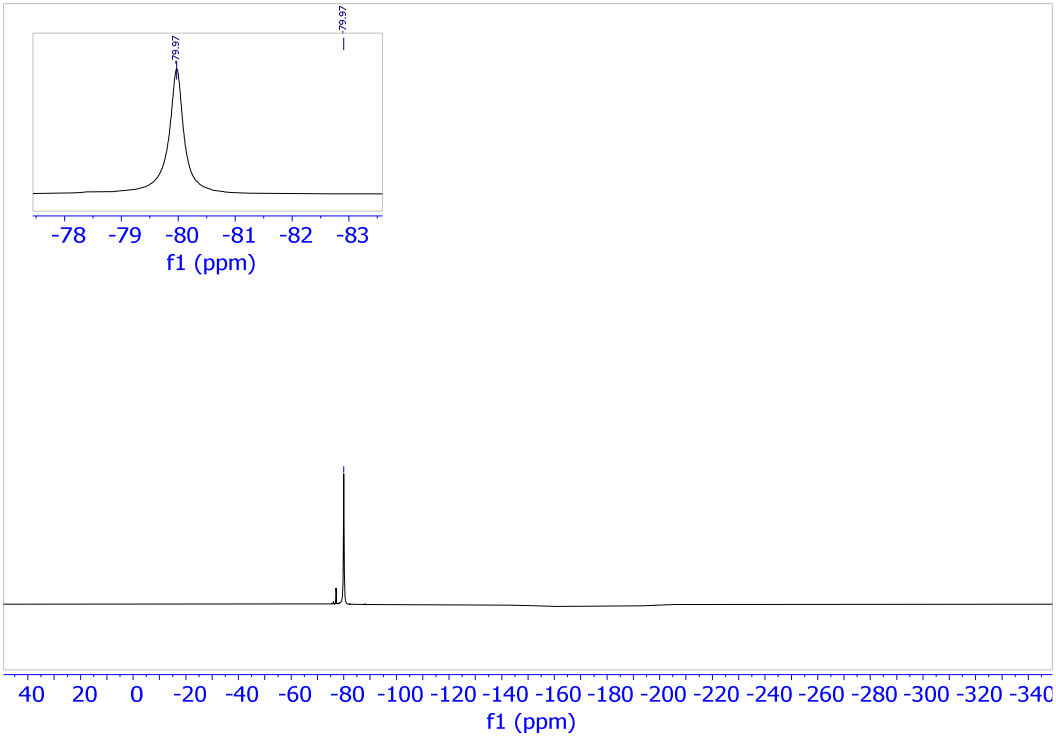

Figure S8. ^{19}F spectrum of **[(*S,S,S*)/(*R,R,R*)-4]** in CD_2Cl_2 at 298 K (376 MHz). Inset: expanded region from -83.5 to -77.4 ppm.

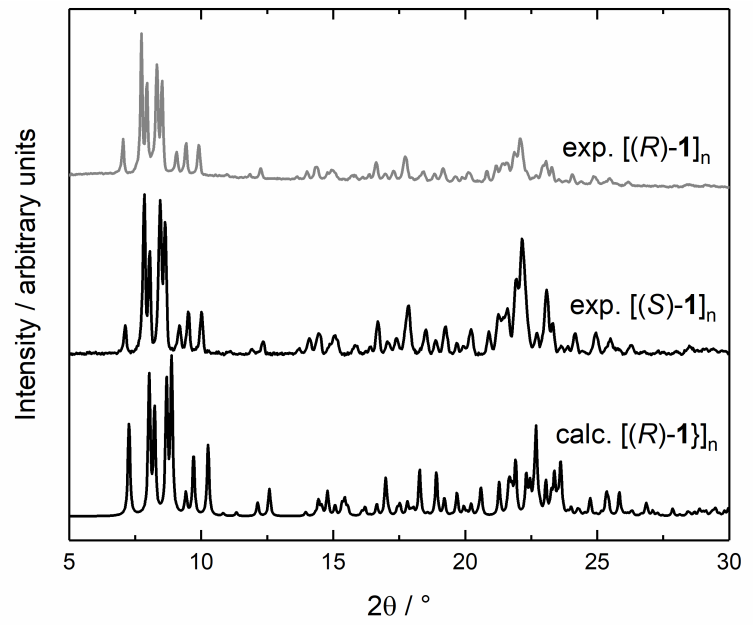

Figure S9. Superposition of experimental powder X-ray diffraction patterns from **[(*S*)-1]$_n$** and **[(*R*)-1]$_n$** measured at 300 K and simulated from **[(*R*)-1]$_n$** single-crystal data obtained at 150 K[2].

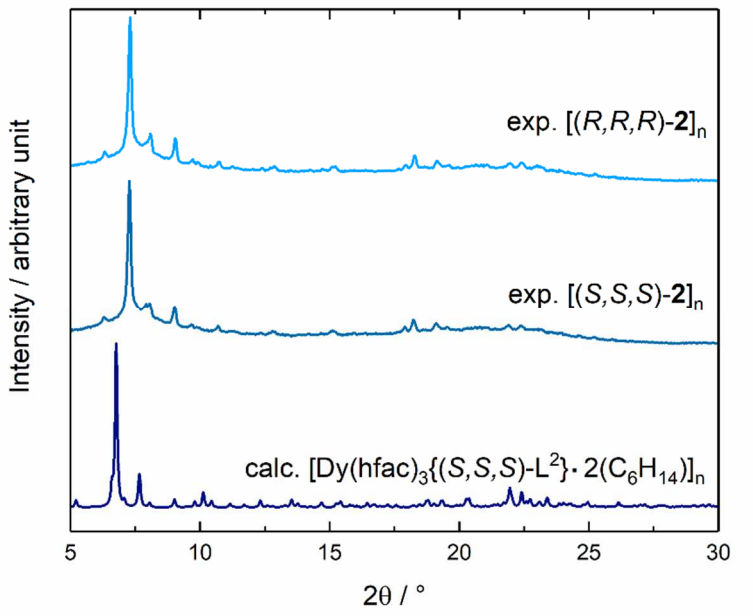

Figure S10. Superposition of experimental powder X-ray diffraction patterns from **[(*S,S,S*)-2]$_n$** and **[(*R,R,R*)-2]$_n$** measured at 300 K and simulated from {[Dy(hfac)$_3$((*S,S,S*)-L^2)]·2(C$_6$H$_{14}$)}$_n$ single-crystal data obtained at 150 K[2].

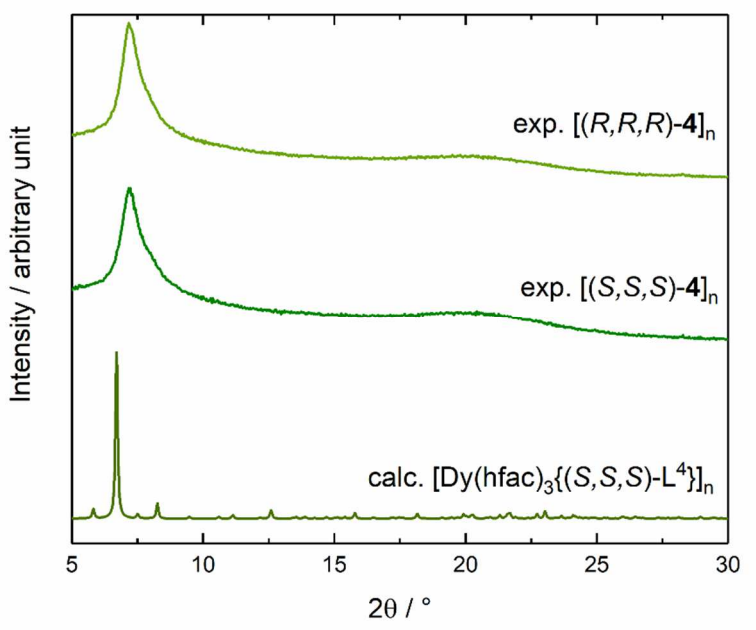

Figure S11. Superposition of experimental powder X-ray diffraction patterns from **[(*S,S,S*)-4]$_n$** and **[(*R,R,R*)-4]$_n$** measured at 300 K and simulated from {[Dy(hfac)$_3$((*S,S,S*)-L^4)]}$_n$ single-crystal data obtained at 150 K[3].

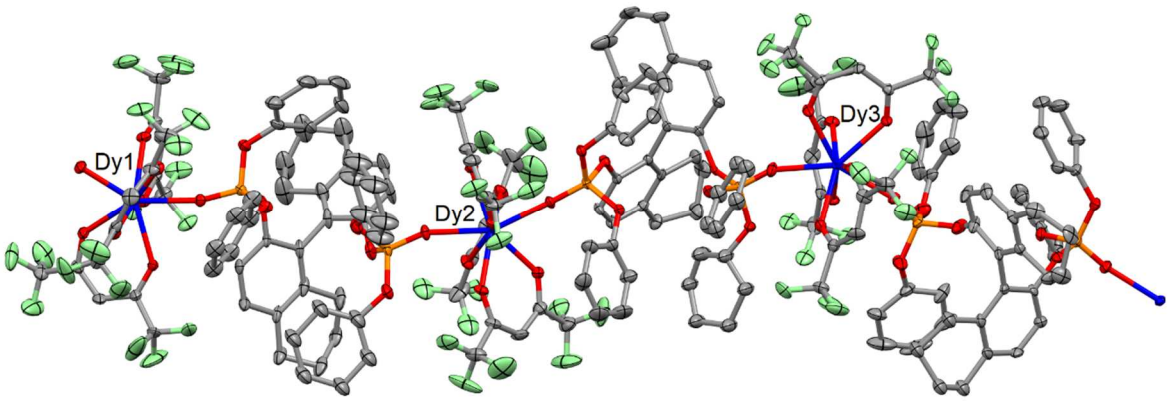

Figure S12. ORTEP view of the asymmetric unit for {[Dy(hfac)$_3$((*S*)-L^3)]}$_n$. Thermal ellipsoids are drawn at 30% probability. Hydrogen atoms are omitted for clarity.

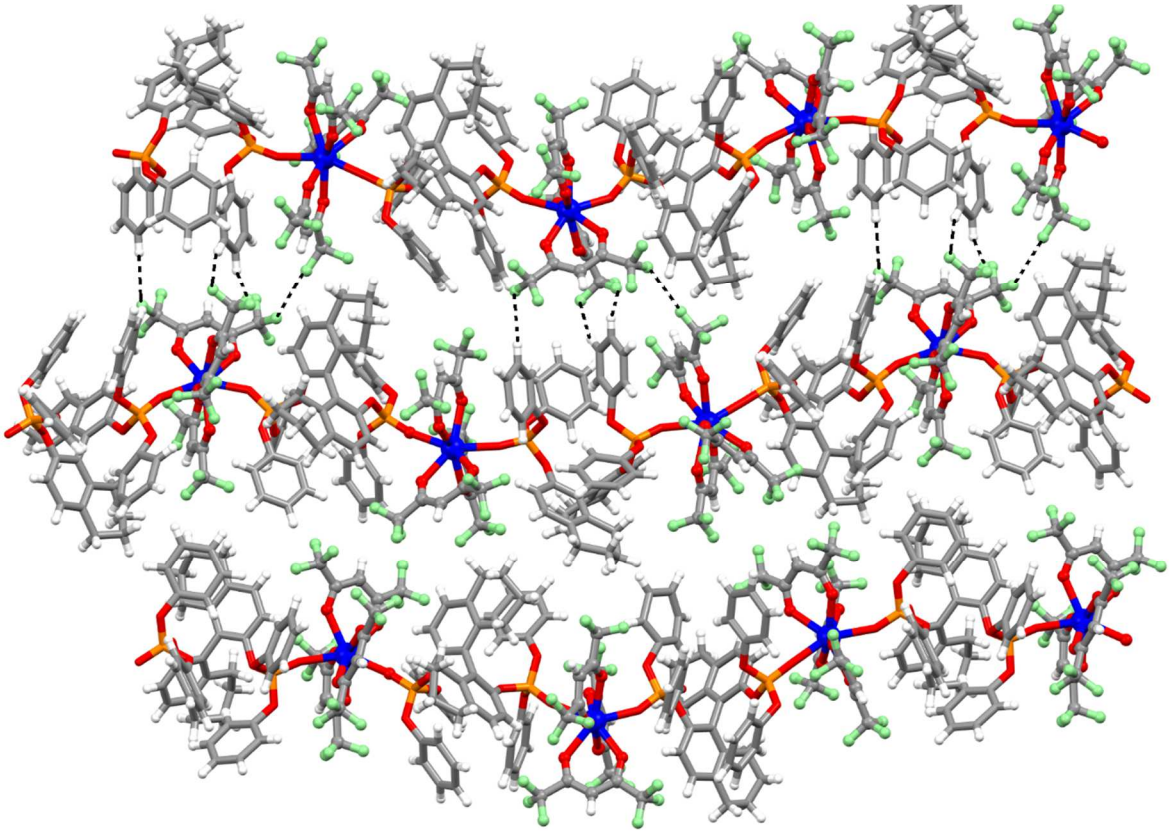

Figure S13. Crystal packing of $\{[Dy(hfac)_3((S)\text{-}L^3)]\}_n$ highlighting the F···F and H···F contacts.

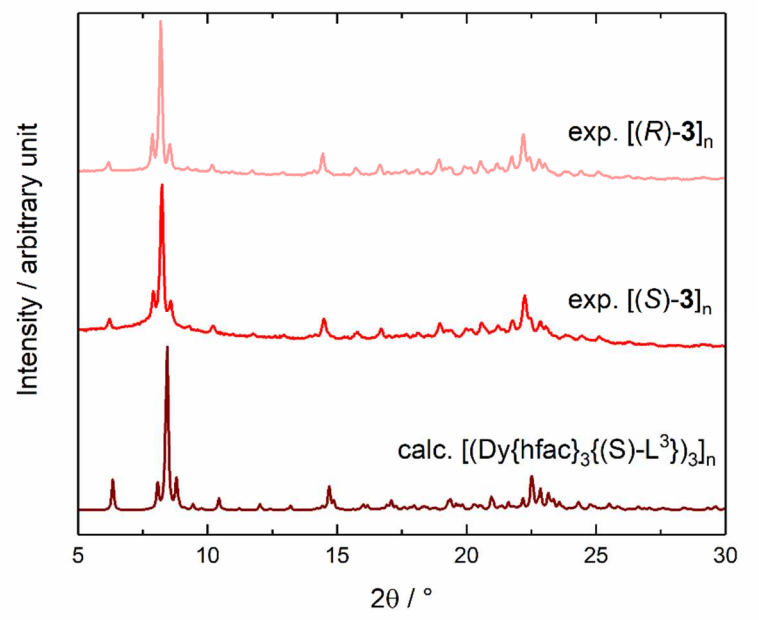

Figure S14. Superposition of experimental powder X-ray diffraction patterns from **[(*S*)-3]$_n$** and **[(*R*)-3]$_n$** measured at 300 K and simulated from $\{[Dy(hfac)_3((S)\text{-}L^3)]_3\}_n$ single-crystal data obtained at 150 K[3].

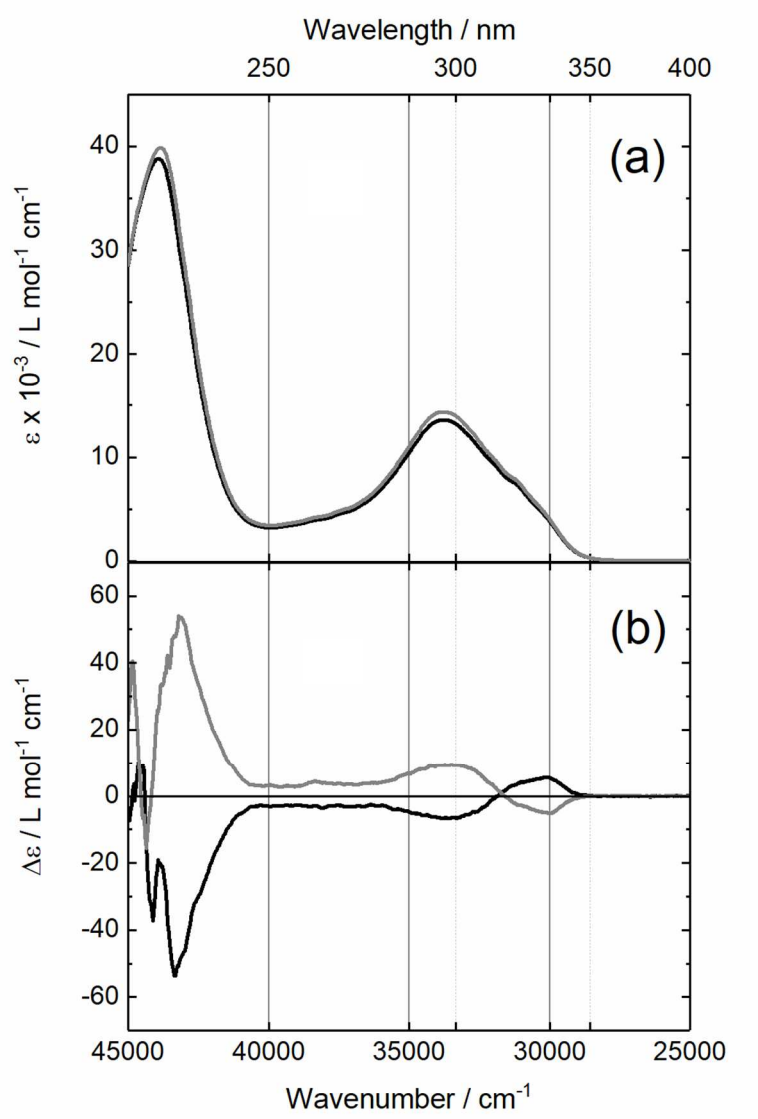

Figure S15. (a) UV-visible absorption and (b) ECD spectra in CH_2Cl_2 solution at $C = 1 \cdot 10^{-5}$ mol L^{-1} and room temperature for **[(*S*)-1]** (gray line) and **[(*R*)-1]** (black line).

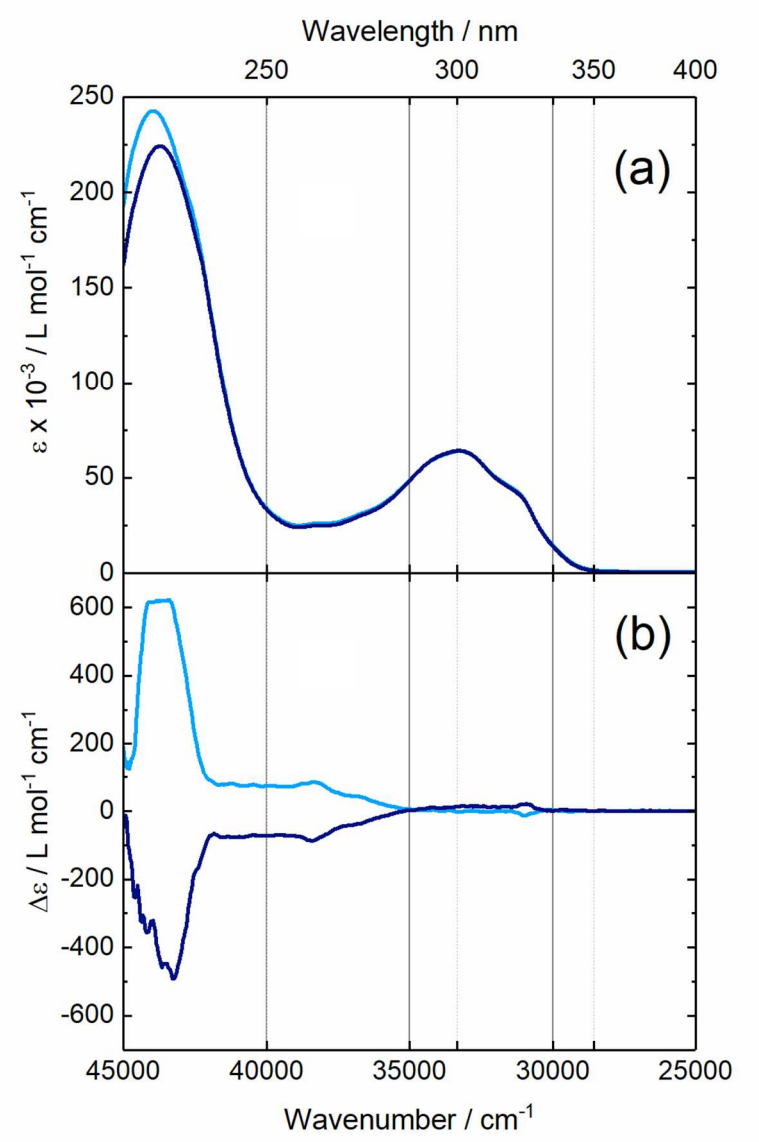

Figure S16. (a) UV-visible absorption and (b) ECD spectra in CH_2Cl_2 solution at C = $1 \cdot 10^{-5}$ mol L^{-1} and room temperature for **[(*S*,*S*,*S*)-2]*** (light blue line) and **[(*R*,*R*,*R*)-2]** (dark blue line). * The ECD signal at low energy is slightly saturated for this compound.

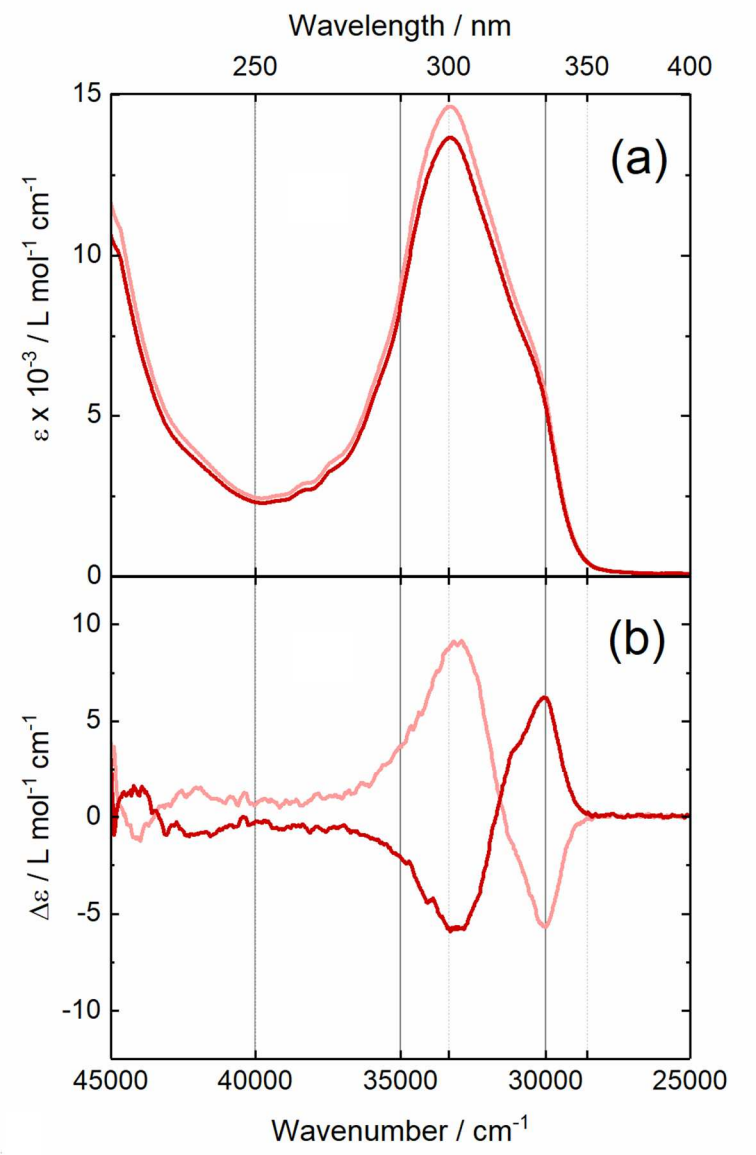

Figure S17. (a) UV-visible absorption and (b) ECD spectra in CH_2Cl_2 solution at C = $1 \cdot 10^{-4}$ mol L^{-1} and room temperature for **[(*S*)-3]** (light red line) and **[(*R*)-3]** (dark red line).

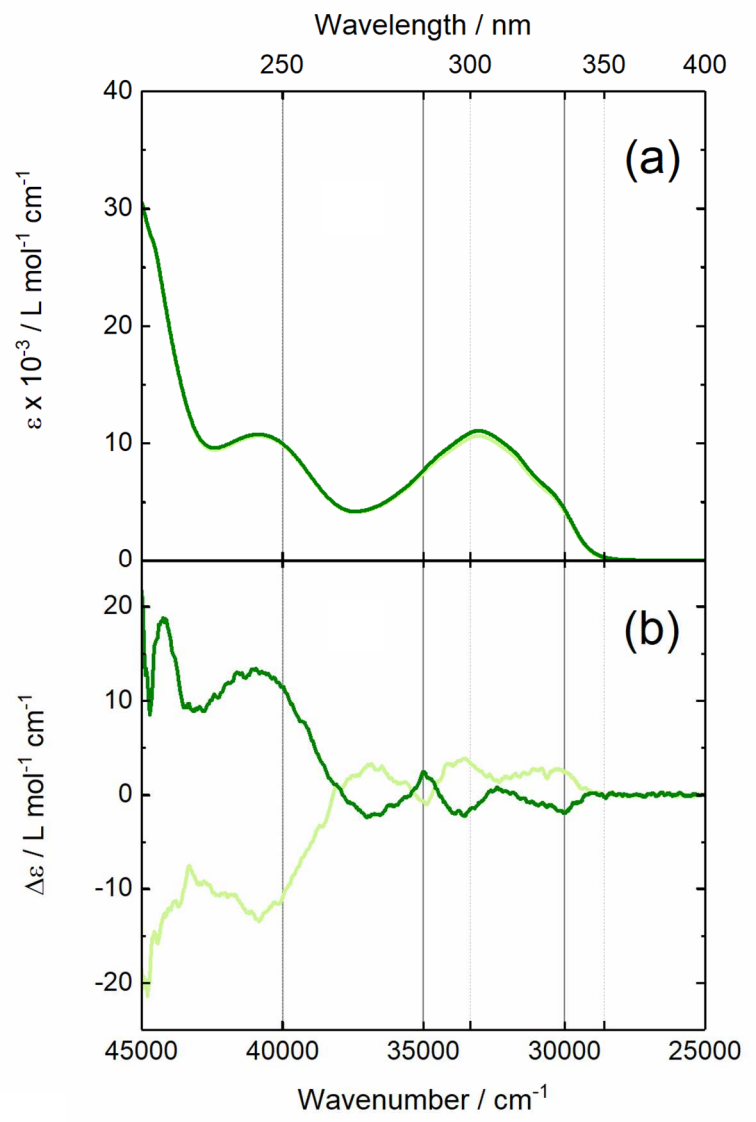

Figure S18. (a) UV-visible absorption and (b) ECD spectra in CH_2Cl_2 solution at C = $5 \cdot 10^{-5}$ mol L^{-1} and room temperature for **[(*S*,*S*,*S*)-4]** (light green line) and **[(*R*,*R*,*R*)-4]** (dark green line).

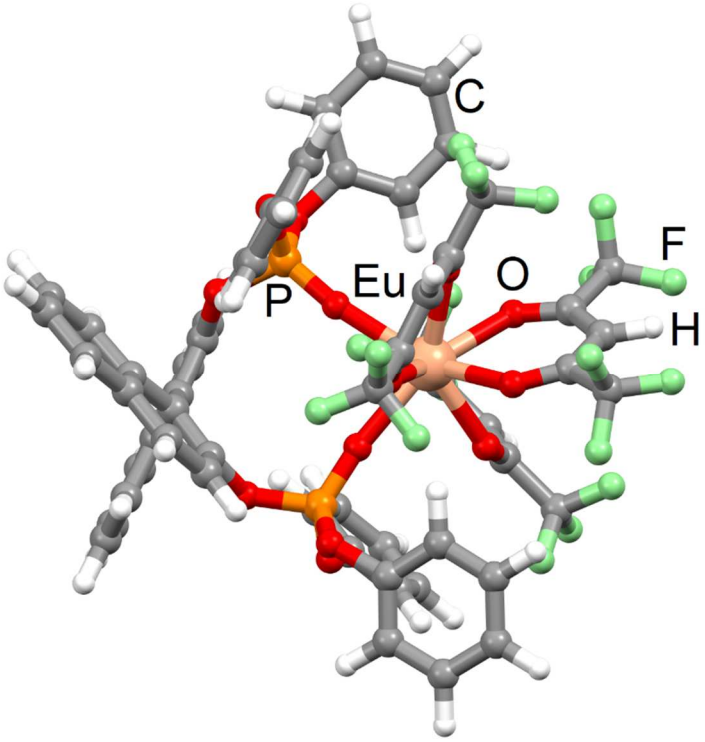

Figure S19. DFT optimized structure of **[(*S*)-1]** expected in CH_2Cl_2 solution.

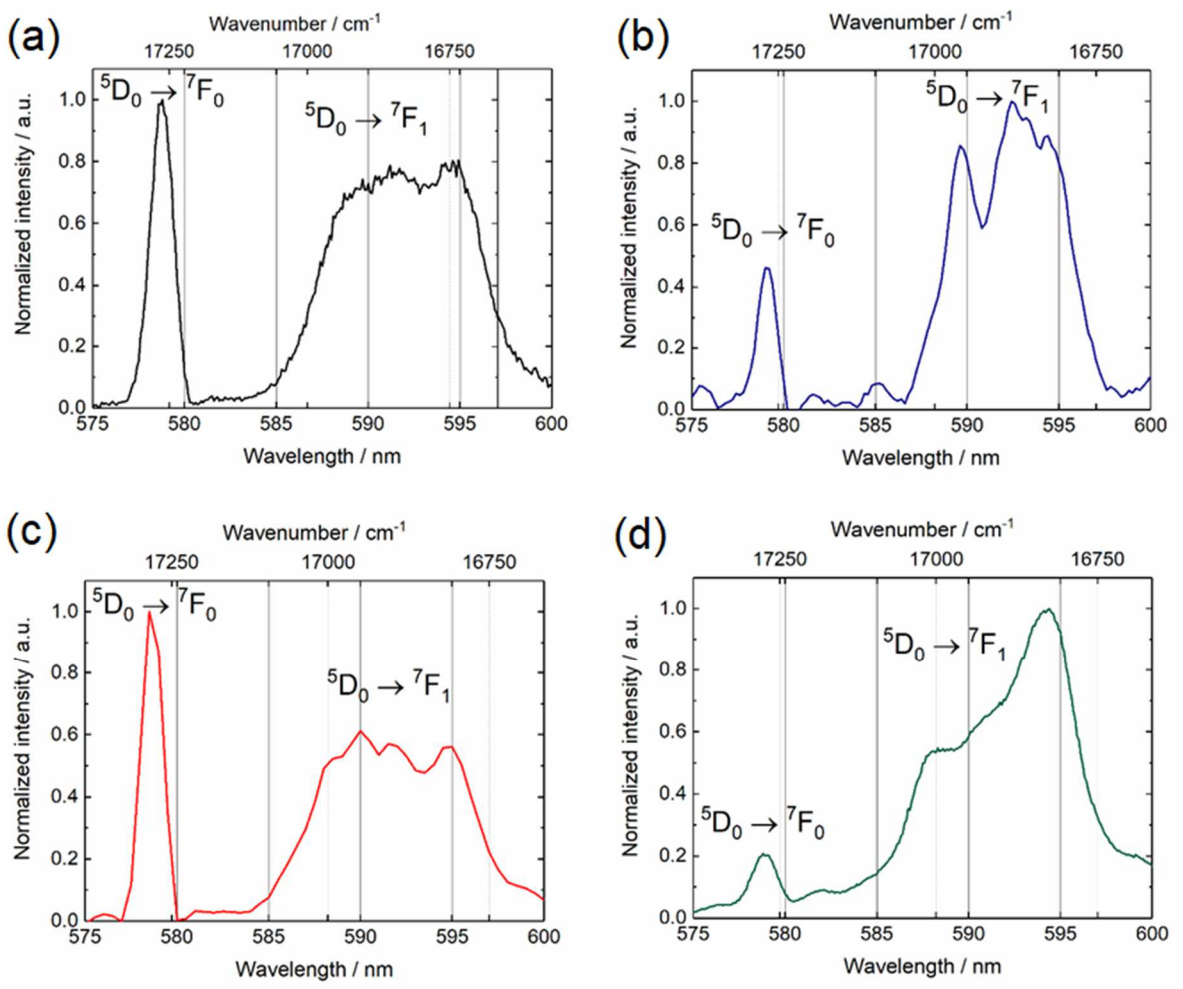

Figure S20. Emission spectra of the $^5D_0 \rightarrow {}^7F_J$ (J = 0,1) transitions measured in CH_2Cl_2 solution under 335 nm (29851 cm^{-1}) irradiation at room temperature for **[(*S/R*)-1]** (a), **[(*S,S,S/R,R,R*)-2]** (b), **[(*S/R*)-3]** (c) and **[(*S,S,S/R,R,R*)-4]** (d).

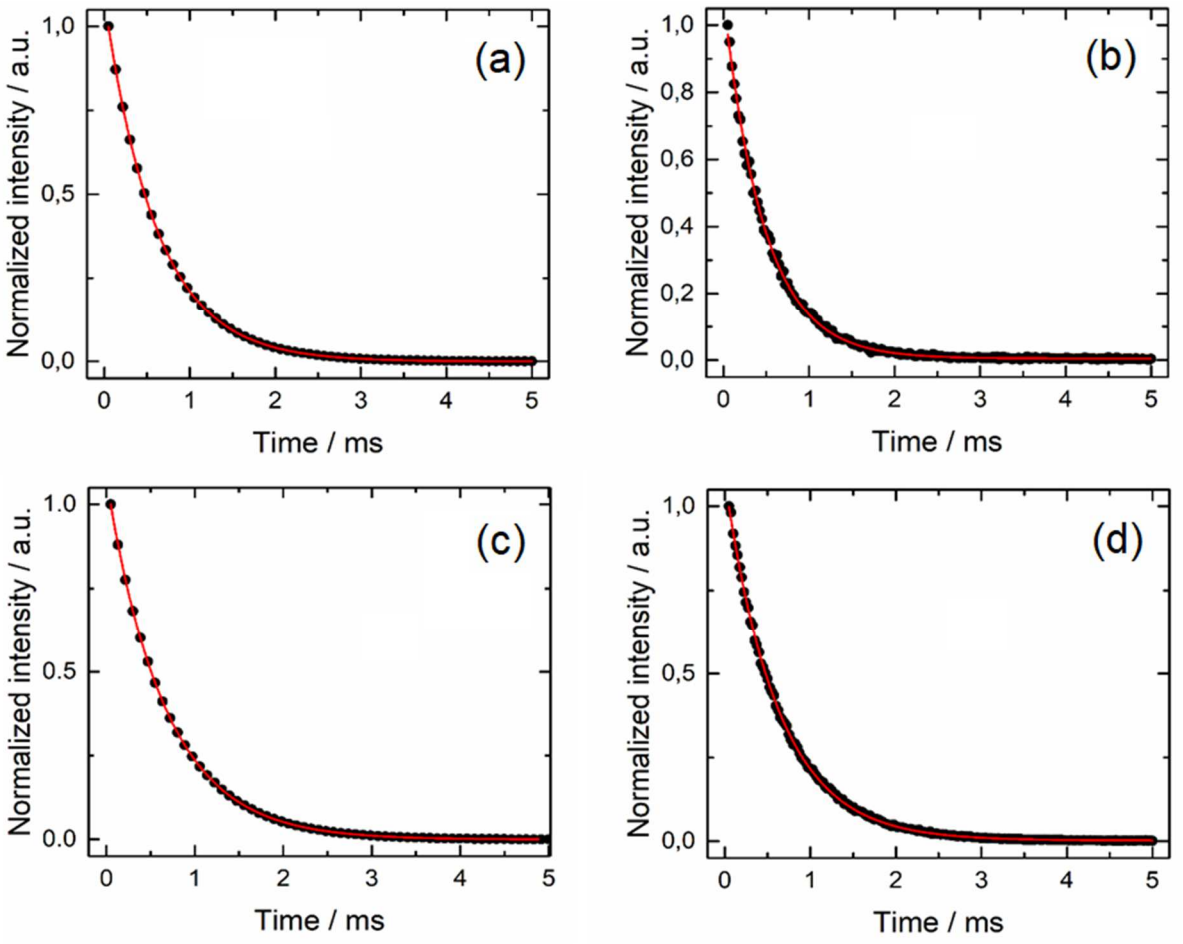

Figure S21. Emission lifetime decays (black dots) and mono-exponential fit curves (red line) for **[(*S/R*)-1]** (a), **[(*S,S,S/R,R,R*)-2]** (b), **[(*S/R*)-3]** (c) and **[(*S,S,S/R,R,R*)-4]** (d) in CH_2Cl_2 solution excited at 330 nm (30303 cm^{-1}).

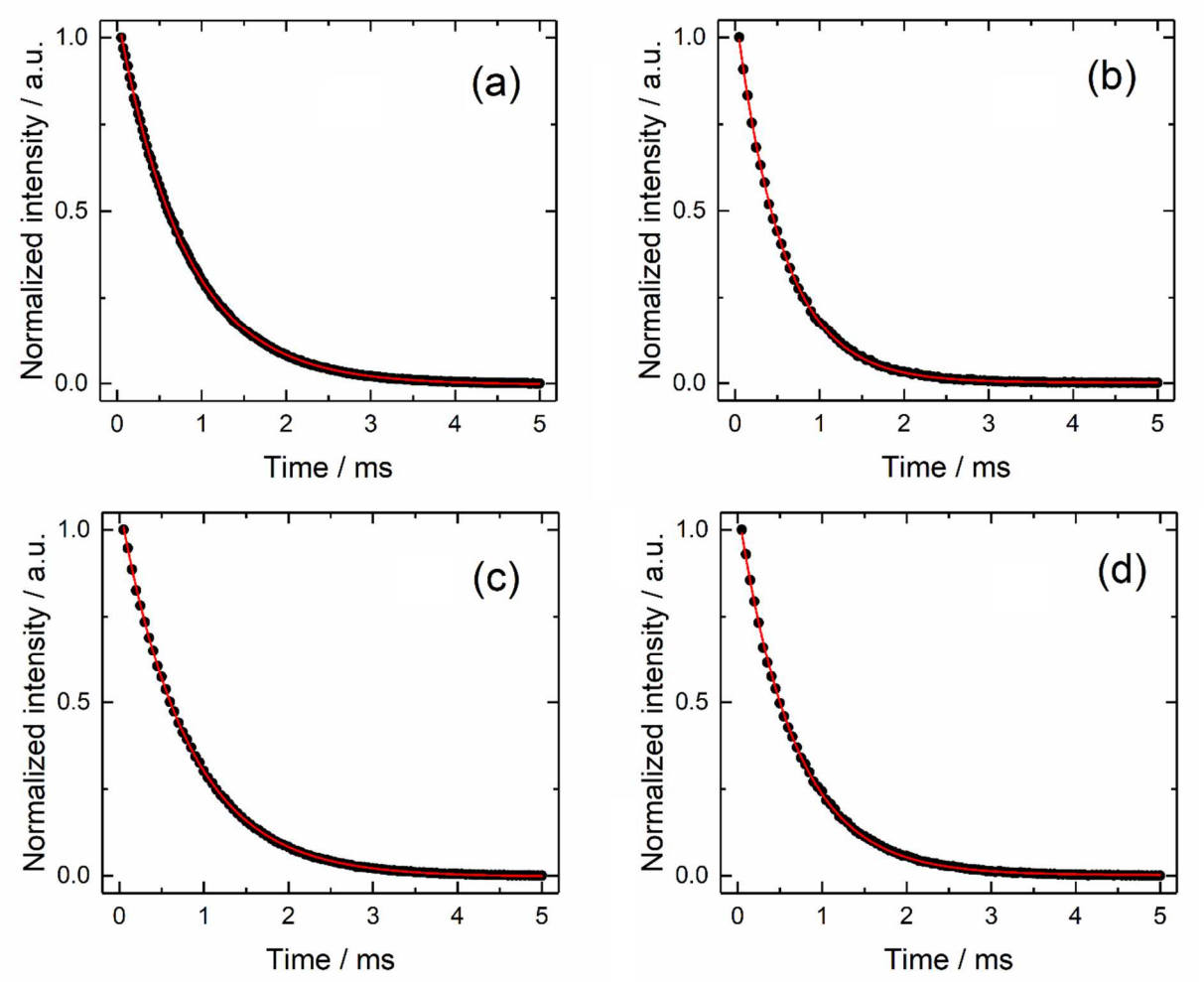

Figure S22. Emission lifetime decays (black dots) and mono-exponential fit curves (red line) for **[(*S/R*)-1]$_n$** (a), **[(*S,S,S/R,R,R*)-2]$_n$** (b), **[(*S/R*)-3]$_n$** (c) and **[(*S,S,S/R,R,R*)-4]$_n$** (d) in solid-state excited at 330 nm (30303 cm^{-1}).

Table S1. Cell parameters for **[(*S,S,S*)-4]$_n$**

Compound	{[Eu(hfac)$_3$((*S,S,S*)-L^4)]}$_n$ **[(*S,S,S*)-4]$_n$**
Formula	$C_{75}H_{63}EuF_{18}O_{14}P_2$
M / g.mol^{-1}	1533
Crystal system	Orthorhombic
Cell parameters	a = 18.853(25) Å b = 18.853 Å c = 26.512(30) Å
Volume / Å^3	9422.9(227)
T / K	150(2)

Table S2. X-ray crystallographic data for {[Dy(hfac)$_3$((*S*)-L^3)]$_3$}$_n$.

Compound	{[Dy(hfac)$_3$((*S*)-L^3)]$_3$}$_n$
Formula	$C_{177}H_{129}Dy_3F_{54}O_{42}P_6$
M / g.mol^{-1}	4627.11
Crystal system	Orthorhombic
Space group	$P2_12_12_1$ (N°19)
Cell parameters	a = 11.9074(5) Å b = 36.1296(16) Å c = 43.7830(18) Å
Volume / Å^3	18835.9(14)
Z	4
T / K	150(2)
2θ range /°	4.20 ≤ 2θ ≤ 55.17
ρ_{calc} / g.cm^{-3}	1.632
μ / mm^{-1}	1.357
Number of reflections	177762
Independent reflections	43311
R_{int}	0.0364
$Fo^2 > 2\sigma(Fo)^2$	39888
Number of variables	2376
R_1, ωR_2	0.0546, 0.1198

Table S3. SHAPE analysis of the coordination polyhedra around the lanthanide in the polymeric compound {[Dy(hfac)$_3$((*S*)-L^3)]$_3$}$_n$.

Compounds	Metal	CShM$_{SAPR-8}$ (square antiprism D_{4d})	CShM$_{BTPR-8}$ (biaugmented trigonal prism C_{2v})	CShM$_{TDD-8}$ (triangular dodecahedron D_{2d})
{[Dy(hfac)$_3$((*S*)-L^3)]$_3$}$_n$	Dy1	0.464	2.745	1.987
	Dy2	1.133	1.923	1.174
	Dy3	0.306	1.623	1.573

Table S4. Selected dissymmetry factors g_{lum} for **[(*S*/*R*)-1]** in CH_2Cl_2 solution at room temperature.

[(*S*)-1]		**[(*R*)-1]**	
wavelength / nm	g_{lum}	wavelength / nm	g_{lum}
587.4	6.4E-03	587.4	-5.2E-03
591.4	4.6E-02	591.4	-4.7E-02
596.0	2.7E-02	596.0	-2.7E-02
611.4	-1.2E-03	611.5	1.7E-03
612.8	-7.9E-04	612.9	7.9E-04
614.5	2.1E-03	614.2	-1.6E-03
619.3	-2.6E-03	619.2	2.1E-03
624.1	-7.4E-03	624.0	6.9E-03
649.5	-2.0E-02	649.5	1.9E-02
652.3	1.6E-02	652.3	-1.5E-02
655.3	6.9E-03	655.3	-5.5E-03
690.1	2.2E-02	690.1	-1.9E-02
696.3	-1.4E-02	696.3	1.7E-02
700.6	7.1E-03	700.6	-6.5E-03
705.4	1.2E-02	705.4	-4.8E-03

Table S5. Selected dissymmetry factors g_{lum} for **[(*S,S,S*/*R,R,R*)-2]** in CH_2Cl_2 solution at room temperature.

[(*S,S,S*)-2]		**[(*R,R,R*)-2]**	
wavelength / nm	g_{lum}	wavelength / nm	g_{lum}
587.0	6.3E-02	587.0	-6.3E-02
594.9	1.2E-01	594.9	-1.1E-01
613.1	-7.1E-03	613.1	7.9E-03
616.1	-1.9E-03	616.1	1.7E-03
619.7	4.4E-03	619.7	-3.0E-03
622.2	-5.4E-03	622.8	8.1E-03
650.0	-1.8E-02	650.0	1.9E-02
651.9	2.5E-02	651.9	-1.9E-02
655.5	5.9E-03	655.5	-7.5E-03
692.0	-9.0E-03	692.0	2.8E-03
696.6	5.1E-03	696.6	-8.5E-03
700.2	-4.5E-03	700.2	4.1E-03

Table S6. Selected dissymmetry factors g_{lum} for **[(*S*/*R*)-3]** in CH_2Cl_2 solution at room temperature.

[(*S*)-3]		**[(*R*)-3]**	
wavelength / nm	g_{lum}	wavelength / nm	g_{lum}
590.0	-5.4E-03	590.0	4.7E-03
592.0	2.8E-02	592.2	-2.8E-02
594.0	-8.8E-03	594.0	9.3E-03
596.4	1.8E-02	596.4	-1.8E-02
611.6	-7.4E-04	611.8	6.4E-04
614.8	1.7E-03	615.0	-2.3E-03
620.4	-2.7E-03	620.6	2.5E-03
624.8	-7.6E-03	625.0	6.8E-03
650.0	-1.4E-02	650.6	1.9E-02
654.0	9.4E-03	654.0	-6.8E-03
691.0	1.6E-02	691.2	-1.8E-02
695.5	-1.4E-02	697.4	1.6E-02
701.0	4.6E-03	701.4	-6.5E-03

Table S7. Selected dissymmetry factors g_{lum} for **[(*S,S,S/R,R,R*)-4]** in CH_2Cl_2 solution at room temperature.

[(*S,S,S*)-4]		**[(*R,R,R*)-4]**	
wavelength / nm	g_{lum}	wavelength / nm	g_{lum}
587.0	2.3E-02	587.0	-2.0E-02
589.7	1.8E-02	589.7	-2.2E-02
594.3	5.3E-02	594.3	-5.3E-02
611.9	-2.7E-03	611.9	3.2E-03
650.9	-7.0E-03	650.9	1.2E-02
652.5	1.6E-02	652.5	-1.4E-02
655.5	7.1E-03	655.5	-2.0E-03
690.5	1.5E-04	690.5	4.3E-03
695.9	7.5E-03	695.9	-8.2E-03
699.0	-3.5E-04	699.0	5.1E-03

Table S8. Experimental lifetime (τ_{obs}) for the europium compounds in solid-state excited at 330 nm (30303 cm^{-1}).

Compounds	τ_{obs} (ms)
	(*S*) or (*S,S,S*)
[**1**]	0.78
[**2**]	0.55
[**3**]	0.80
[**4**]	0.66

Table S9. Selected dissymmetry factors g_{lum} for **[(*S/R*)-1]$_n$** in solid-state at room temperature.

[(*S*)-1]$_n$		**[(*R*)-1]$_n$**	
wavelength / nm	g_{lum}	wavelength / nm	g_{lum}
587.4	5.7E-03	587.4	-5.7E-03
594.7	2.6E-02	594.7	-2.2E-02
613.4	-4.9E-03	613.4	4.6E-03
617.1	-1.4E-03	617.1	1.1E-03
621.3	5.1E-03	621.3	-4.7E-03
649.5	-1.9E-02	649.5	2.1E-02
651.3	2.9E-03	651.3	-2.9E-03
652.9	-8.5E-03	652.9	1.3E-02
655.1	7.0E-03	655.1	-5.3E-03
690.9	4.3E-03	690.9	-3.6E-03
695.7	-4.3E-03	695.7	4.1E-03
698.7	5.1E-03	698.7	-5.0E-03
701.4	-6.7E-04	701.4	5.3E-03

Table S10. Selected dissymmetry factors g_{lum} for **[(*S,S,S/R,R,R*)-2]$_n$** in solid-state at room temperature.

[(*S,S,S*)-2]$_n$		**[(*R,R,R*)-2]$_n$**	
wavelength / nm	g_{lum}	wavelength / nm	g_{lum}
587.2	-5.5E-03	586.4	6.4E-03
595.3	-1.3E-02	594.6	1.8E-02
610.5	1.7E-03	613.6	-3.4E-03
612.8	2.1E-03	612.8	-1.8E-03
615.8	1.2E-03	615.3	-1.8E-03
621.5	-2.3E-03	621.3	3.6E-03
648.9	7.5E-03	649.4	-1.6E-02

Table S11. Selected dissymmetry factors g_{lum} for **[(*S/R*)-3]$_n$** in solid-state at room temperature.

[(*S*)-3]$_n$		**[(*R*)-3]$_n$**	
wavelength / nm	g_{lum}	wavelength / nm	g_{lum}
587.2	-3.8E-03	587.5	3.5E-03
591.8	2.8E-02	591.5	-2.8E-02
595.4	-1.6E-02	595.4	1.3E-02
612.5	8.9E-04	612.5	-8.9E-04
614.0	-1.4E-03	613.8	1.1E-03
616.8	1.3E-03	617.0	-8.5E-04
621.5	-5.8E-04	621.0	5.6E-04
623.0	1.5E-03	623.3	-9.0E-04
649.6	7.6E-03	649.6	-7.9E-03
651.5	-4.7E-03	651.5	4.6E-03

Table S12. Selected dissymmetry factors g_{lum} for **[(*S,S,S/R,R,R*)-4]$_n$** in solid-state at room temperature.

[(*S,S,S*)-4]$_n$		**[(*R,R,R*)-4}]$_n$**	
wavelength / nm	g_{lum}	wavelength / nm	g_{lum}
587.0	-1.5E-02	587.0	1.3E-02
590.8	9.5E-03	590.8	-9.1E-03
594.7	-2.5E-02	594.7	2.3E-02
612.9	4.9E-03	612.9	-2.9E-03
617.5	3.1E-03	617.5	-1.7E-03
621.5	-4.1E-03	621.5	4.6E-03
649.3	1.7E-02	649.3	-1.3E-02
651.5	-4.2E-03	651.5	2.9E-03
655.5	2.4E-03	655.5	-2.6E-04

References

1. Llunell M, Casanova D, Cirera J, Alemany P, Alvarez, S. SHAPE Program for the Stereochemical Analysis of Molecular Fragments by Means of Continuous Shape Measures and Associated Tools, Departament de Quimica Fisica, Departament de Quimica Inorganica,and Institut de Quimica Teorica i Computacional – Universitat dè Barcelona, Barcelona, Spain.
2. Mattei CA, Montigaud V, Gendron F, et al. Solid-state versus solution investigation of a luminescent chiral BINOL-derived bisphosphate single-molecule magnet. *Inorg Chem Front.* 2021;8:947-962.
3. Mattei CA, Montigaud V, Dorcet V, et al. Luminescent dysprosium single-molecule magnets made from designed chiral BINOL-derived bisphosphate ligands. *Inorg Chem Front.* 2021;8:963-976.